

Satellite image deblurring using complex wavelet packets

André Jalobeanu, Laure Blanc-Féraud, Josiane Zerubia

Abstract

The deconvolution of blurred and noisy satellite images is an ill-posed inverse problem. Direct inversion leads to unacceptable noise amplification. Usually the problem is regularized during the inversion process. Recently, new approaches have been proposed, in which a rough deconvolution is followed by noise filtering in the wavelet transform domain. Herein, we have developed this second solution, by thresholding the coefficients of a new complex wavelet packet transform; all the parameters are automatically estimated. The use of complex wavelet packets enables translational invariance and improves directional selectivity, while remaining of complexity $O(N)$. A new hybrid thresholding technique leads to high quality results, which exhibit both correctly restored textures and a high SNR in homogeneous areas. Compared to previous algorithms, the proposed method is faster, rotationally invariant and better takes into account the directions of the details and textures of the image, improving restoration. The images deconvolved in this way can be used as they are (the restoration step proposed here can be inserted directly in the acquisition chain), and they can also provide a starting point for an adaptive regularization method, enabling one to obtain sharper edges.

I. INTRODUCTION

The problem presented here is the reconstruction of a satellite image from blurred and noisy data.

The degradation model is represented by the equation :

$$Y = H\mathcal{X} + N \quad \text{where} \quad H\mathcal{X} = h \star \mathcal{X} \quad (1)$$

Y is the observed data and \mathcal{X} the original image. N is additive noise and is assumed to be Gaussian, white and stationary. The \star represents a circular convolution. The Point Spread Function (PSF) h is positive. We assume there is no spectral overlapping. We deal with a real satellite image deblurring problem, proposed by the French Space Agency (CNES). This problem is part of a simulation of the SPOT 5 satellite. The noise standard deviation σ and the PSF h are assumed known.

The deconvolution problem is ill-posed because of the noise, which contaminates the data. The inversion process strongly amplifies the noise if no regularization is done. Thus, we have to deconvolve the observed image while recovering the details, but without amplifying the noise.

The process used to estimate \mathcal{X} from the degraded data Y must preserve the textures, enabling us to obtain visually correct results. Moreover, the noise should remain small in homogeneous regions. Many methods have been proposed for regularizing this problem by introducing a priori constraints on the solution [4], [11], [26], [28]. However, most of them do not preserve textures, since these textures are not taken into account in the regularizing model. To achieve a better deconvolution, other authors [1], [22], [24] prefer to use a wavelet-based regularizing function. However, all these approaches have the drawback that they are iterative, which means that they are time consuming and not always appropriate for deconvolving satellite data, where the images can be very large.

A few authors, such as Donoho et al. [8], proposed to deblur signals in a wavelet-vaguelette basis. Rougé [25], then Mallat and Kalifa [18], proposed to denoise images after a *deconvolution without regularization*, in order to perform a fast and noise-free deconvolution. All these techniques can be summarized by the following two steps: deconvolution by a pseudo-inverse or generalized inverse filter, and denoising. In the second step, the images are represented using a wavelet packet basis, and the denoising process is done in this basis, by thresholding the noisy coefficients. This type of method is not iterative and provides a very fast implementation.

A simple inversion of the observation equation (1) in frequency space gives an unacceptably noisy solution. To denoise it, a sparse representation has to be chosen, in order to separate the signal from the noise as well as possible. A representation is said to be sparse if it approximates the signal with a small number of parameters, which can be the coefficients of the decomposition in a given basis.

The noise amplified by the deconvolution process is colored. Furthermore, the coefficients of this noise are not independent in the wavelet basis. Thus, the basis must adapt to the covariance properties of the noise. The covariance matrix should be *nearly diagonal* [17] in the basis, to decorrelate the noise coefficients as much as possible. The Fourier basis achieves such a diagonalization, but the energy of the signal is not concentrated over a small number of coefficients (the basis vectors are not spatially localized), so the Fourier transform is not suitable for any thresholding method.

A good compromise is to use a *wavelet packet* basis [6], since it nearly realizes the two following essential conditions, i.e. the signal representation is sparse, and the noise covariance operator is nearly diagonalized [17].

Many types of wavelets transforms can be used to construct a packet basis; they exhibit different properties depending on their spatial or frequency localization, and on their separability w.r.t. rows and columns. Decimated real wavelet transforms are efficient for satellite image deconvolution but produce artefacts since the transform is not shift invariant. It is well known that to avoid these artefacts, the resulting image may be averaged over all possible integer translations [5]. It is also possible to use shift invariant transforms, but the redundancy is generally rather high and depends on the depth of the transform. These two techniques have the major drawback of slowing down the algorithm.

The main motivation of our work is to solve this problem in a computationally efficient manner. There is a way to enable translation invariance without much loss of computational time, by using complex wavelets [19], [20]. Such wavelets also provide a better restoration by separating 6 directions, while real separable wavelets only take into account two directions. In order to achieve the necessary near-diagonalization of the deconvolved noise covariance, we have implemented a *complex wavelet packet* algorithm.

Our essential contributions are the following :

1. We have designed a new transform, the complex wavelet packet transform, which has better directional selectivity than the complex wavelet transform, while exhibiting the same shift invariance properties. This is illustrated by Fig. 1.

2. The proposed algorithm is fully automatic, since it is based on a Bayesian approach, where all the necessary parameters are estimated from the observed data.
3. We have proposed a new hybrid technique, consisting of combining two different methods, regularization and wavelet thresholding, to obtain optimal deconvolution results.
4. It performs the inversion faster than shift invariant real transforms and reconstructs features with dominant diagonal orientations better.

The paper is organized as follows. First, in section II, we detail how to compute the proposed complex wavelet packet transform and the properties of this new transform. Then, in section III, we present the Bayesian thresholding framework used to estimate the unknown coefficients from the observed data, and explain how to compute the variance of the deconvolved noise. In section III-A, we describe the observation model and the Bayesian framework. The proposed adaptive prior model of the wavelet coefficients is presented in section III-B. In section III-C, we detail the new hybrid technique used to estimate the adaptive parameters of the former. Section III-D is devoted to the hyperprior put on the parameters of the prior distribution. The proposed algorithm is described in section IV. Finally, we present, in section V, a comparison with classical algorithms used for satellite image deconvolution, to demonstrate the effectiveness of the proposed method.

II. COMPLEX WAVELET PACKET TRANSFORM (CWPT)

This new transform is built in order to take advantage of the packet decomposition and the interesting properties of the complex wavelet transform at the same time.

A. Implementation

To build a complex wavelet transform, Kingsbury [19] has developed a quad-tree algorithm, by noting that an approximate shift invariance can be obtained with a real biorthogonal transform by doubling the sampling rate at each scale. This is achieved by computing 4 parallel wavelet transforms, which are differently subsampled. Thus, the redundancy is limited to 4, compared to real shift invariant transforms.

Therefore, it involves two pairs of biorthogonal filters, odd, h^o and g^o , and even, h^e and g^e . At level $j = 1$, it is simply a non-decimated wavelet transform (using h^o and g^o) whose coefficients are re-ordered into 4 interleaved images by using their parity. This defines the 4 trees $T=A, B, C$ and D . For $j > 1$, each tree is processed separately, as a real transform, with a combination of odd and even filters depending on each tree. The transform is

achieved by a fast filter bank technique, of complexity $O(N)$. The reconstruction is done in each tree independently, by using the dual filters, and the results of the 4 trees are averaged to obtain a^0 to ensure the symmetry between the trees, thus enabling the desired shift invariance.

The complex coefficients are obtained by combining the different trees together. If we index the subbands by k , the detail subbands $d^{j,k}$ of the parallel trees A , B , C and D are combined to form complex subbands $z_+^{j,k}$ and $z_-^{j,k}$, by the linear transform:

$$\begin{aligned} z_+^{j,k} &= (d_A^{j,k} - d_D^{j,k}) + i(d_B^{j,k} + d_C^{j,k}) \\ z_-^{j,k} &= (d_A^{j,k} + d_D^{j,k}) + i(d_B^{j,k} - d_C^{j,k}) \end{aligned} \quad (2)$$

Thresholding the magnitudes $|z_\pm|$ without modifying the phase enables us to define a nearly shift invariant filtering method.

We have extended the original transform by applying the filters h and g on the detail subbands, thus defining the CWPT. [15], [16]. This enables us to preserve the properties of the original complex wavelet transform. The tree corresponding to the CWP transform is given in Fig. 2.

The filter bank used for the decomposition is illustrated by Fig. 3, on which the subbands are indexed by (p, q) for each tree T . Instead of dividing an approximation space which does not define any new orientation, the wavelet packet decomposition processes the detail subbands, which are strongly oriented. Each detail subband at level 1 isolates an area of the frequency space defined by a mean direction and a dispersion, enabling one to select a range of directions around a given orientation. If the subband is decomposed into 4 new subbands, it means that the corresponding frequency area is split into 4 new areas, which define new orientations, as shown in Fig. 4.

B. Invariance properties

Let us first focus on the properties of the CWPT. The proposed transform enables us to keep the shift invariance properties, as illustrated by Fig. 1. This can be demonstrated in the following way: we perform the CWP transform of a step function (1D signal), we keep only one wavelet packet subband at level 2 (the other subbands are set to zero), and we do the inverse transform. This is done for 4 possible shifts of the input signal, and we remark the approximate shift invariance of the output, for both wavelet packet subbands. This property has already been shown for the complex wavelets for any level j by Kingsbury [21].

The shift invariance is perfect at level 1, and approximately achieved beyond this level: the transform algorithm is designed to optimize the translation invariance.

The impulse responses, shown in Fig. 5, and the related partitioning of the frequency space given in Fig. 4, demonstrate the ability to separate up to 26 directions for the chosen wavelet packet tree. Compared to real separable transforms, which only define two directions (rows and columns), it provides near rotational invariance and gives a selectivity which better represents strongly oriented textures (thus separating them better from the noise). Furthermore, compared to the original complex wavelet transform, which only separates 6 directions, the directional selectivity is highly improved.

The redundancy of the CWPT is the same as the CWT, and this is independent on the decomposition tree. Moreover, the proposed transform remains fully invertible, which makes it usable for deconvolution tasks.

However, this is not really a complex transform, since it is not based on a continuous complex mother wavelet. Nevertheless, the quad-tree transform has in practice the same properties as a complex transform w.r.t. shifting of the input image.

III. BAYESIAN THRESHOLDING

A. The observation model and the Bayesian approach

Let us denote X the deconvolved image without regularization. For each subband k , the variables x and ξ denote one of the CWP coefficients corresponding respectively to the observation Y and the original image \mathcal{X} . We suppose that H is invertible (i.e. it has no zeros in the Fourier space). Since the noise N is white and Gaussian, Eqn. (1) multiplied by H^{-1} gives, in the CWP domain:

$$x = \xi + n \tag{3}$$

To obtain the expression of the noise coefficients n , let us recall Eqn. (2). Each complex coefficient is obtained by summing or subtracting the coefficients of the 4 trees A, B, C, D. If we compute the covariance between the real and imaginary parts, we find (for the coefficients z_+) $E[n_r n_i] = E[n_A n_B + n_A n_C - n_D n_B - n_D n_C]$ where n_A, n_B, n_C, n_D , are the noise coefficients for each tree. By symmetry assumptions, this covariance is null, since all covariances $E[n_T n_{T'}]$ between different trees T and T' are equal. Then, the distribution

of the noise is defined as a joint distribution of (n_r, n_i) :

$$P(n) = \frac{1}{2\pi \sigma_k^2} e^{-|n|^2/2\sigma_k^2}$$

We assume that the noise variance is constant in each subband k . We compute σ_k by using the impulse responses W^k of the subbands. To obtain W^k , we take the CWPT of a discrete Dirac and we keep only the subband k , all the others being set to zero, then we perform the inverse transform. The mean power spectrum of the deconvolved noise is given by $|1/\mathcal{F}[h]|^2$ where \mathcal{F} denotes the Fourier transform. Then, for subband k we have:

$$\sigma_k^2 = \sigma^2 \sum_{ij} \left| \frac{\mathcal{F}[W^k]_{ij}}{\mathcal{F}[h]_{ij}} \right|^2 \quad (4)$$

We assume that the coefficients ξ are independent in a given subband, between different subbands of a given scale, and also between scales. This is an approximation which leads to a fast thresholding technique: we will not handle here possible correlations between subbands or neighbour coefficients. The covariance matrix of the noise is supposed to be nearly diagonal in the chosen basis (see Fig. 6 and Fig. 7), so we consider that the noise variables are also independent in the wavelet packet basis.

We estimate the unknown coefficients ξ within a Bayesian framework [27]. We have shown in [16] that this approach provides slightly better results than the Minimax [9] risk calculus on real satellite data. To compute the MAP estimate of ξ , we use Bayes law to calculate the expression of the posterior probability:

$$\hat{\xi} = \arg \max_{\xi} P(\xi | x) = \arg \max_{\xi} P(x | \xi)P(\xi) \quad (5)$$

where $P(x | \xi)$ is given by the distribution of the noise:

$$P(x | \xi) = \frac{1}{2\pi \sigma_k^2} e^{-|x-\xi|^2/2\sigma_k^2} \quad (6)$$

B. The prior model

The Generalized Gaussian distribution has been used to model the distribution of real wavelet coefficients in each subband [23], [27]. It is also possible to use it to model the CWP subbands. It corresponds to the following prior probability of ξ :

$$P(\xi) = \frac{1}{Z(\alpha_k, p_k)} e^{-|\xi/\alpha_k|^p} \quad (7)$$

where α_k is a prior parameter and p is an exponent, which is supposed to be independent of the subband. We assume that the variables ξ are independent within a given subband,

and also between the different subbands. As shown by Fig. 8, the complex density is a bidimensional function which only depends on the magnitude (it exhibits a radial symmetry). It is generally not separable for $p \neq 2$. The magnitude is governed by a decreasing density function, while the phase is uniformly distributed in $[0, 2\pi)$.

This is a marginal model, which seems to describe a whole subband efficiently, but fails to capture the non stationarity property related to satellite or aerial images. Indeed, all the coefficients of one subband are described by the same distribution with the same set of parameters. If we want to take into account the non stationarity explicitly, it is better to use an adaptive model.

B.1 Inhomogeneous prior model

Another possible way to capture the heavy-tailed behaviour of the subband densities is to define an inhomogeneous model, which adapts to the local characteristics of the subbands. Some approaches to spatial adaptivity in the real wavelet domain can be found in the literature, for example [3].

To simplify, let us choose a Gaussian model. The variance parameter is different for each coefficient, which enables us to differentiate edges or textures, which have a high intensity, from the homogeneous areas which generally correspond to very low values of the coefficients.

Since the parameters can be very different from one variable to another, the histogram of a subband can have a heavy-tailed behaviour, even if the distribution of each variable is Gaussian.

We denote by s^2 the variance parameter of each original coefficient ξ . We propose to use the adaptive prior distribution:

$$P(\xi | s) = \frac{1}{2\pi s^2} e^{-|\xi|^2/2s^2} \quad (8)$$

If the parameters s^2 are known, the unknown wavelet coefficients can be estimated by computing the MAP or the MMSE, which have the same expression in this case. This is a fully Bayesian technique (we use the property (5)). Recall the expression of the noise distribution (6), and combine it with Eqn. (8) to obtain:

$$P(\xi | x) \propto e^{-|x-\xi|^2/2\sigma_k^2 - |\xi|^2/2s^2} \quad (9)$$

Therefore, the MAP is given by:

$$\hat{\xi} = \arg \min_{\xi} \left[\frac{|x - \xi|^2}{2\sigma_k^2} + \frac{|\xi|^2}{2s^2} \right]$$

To compute the minimum, differentiate w.r.t. the real and the imaginary parts of ξ . This gives two equations which are recombined to form an equation with complex numbers:

$$\begin{cases} \frac{\xi_r - x_r}{\sigma_k^2} + \frac{\xi_r}{s^2} = 0 \\ \frac{\xi_i - x_i}{\sigma_k^2} + \frac{\xi_i}{s^2} = 0 \end{cases} \Leftrightarrow \frac{\xi - x}{\sigma_k^2} + \frac{\xi}{s^2} = 0$$

This gives the inhomogeneous MAP estimate:

$$\hat{\xi} = \frac{s^2}{s^2 + \sigma_k^2} x \quad (10)$$

C. Robust parameter estimation

In this paragraph, we focus on the estimation of the adaptive parameters s using the MAP. If we don't use any prior density for these parameters (i.e. we assume there is a flat hyperprior), the MAP estimator reduces to the MLE.

As is shown in [14], the MLE is not robust when applied to incomplete data (i.e. when the estimation is made on noisy data). Indeed, there are as many parameters as observed data. Even if the robustness is insufficient in the incomplete data case, and blurred data, it becomes sufficient when the estimation is made from the original image \mathcal{X} (i.e. complete data). Since this image is unknown, a good approximation of it has to be determined. Then, it is possible to get very useful parameter estimates by using this approximation instead of the original image. Here, we use this complete data approach to estimate the unknown parameters.

Consider Eqn. (8). The complete data MLE is defined by $\hat{s}^2 = \arg \max_{s^2} P(\xi | s^2)$. Assuming independence, we obtain:

$$\hat{s}^2 = \frac{|\xi|^2}{2} \quad (11)$$

where the factor 2 comes from the dimensionality of the distribution.

We obviously do not have access to the original coefficients. That is why we take the transform coefficients of an approximate original image instead. Experiments have shown that a satisfactory approximation is provided by a nonlinear regularizing algorithm, such as RHEA, detailed in [13]. It essentially consists of a variational method based on φ -functions [4] (minimization of a criterion which penalizes noisy solutions, but preserves

the edges) preceded by an automatic parameter estimation step to compute the parameters of the regularizing model.

The proposed algorithm consists of obtaining the desired approximate original image using a method like RHEA [13], estimating the adaptive parameters using the complete data MLE with Eqn. (11), and then estimating the unknown coefficients by computing the MAP by Eqn. (10).

Let us denote by $\tilde{\xi}$ the transform coefficients of the approximate original image. $\tilde{\xi}$ is supposed to be sufficiently noise-free and to contain sufficient information to enable texture and edge recovery.

The restored edges are sharp, since we have used an edge-preserving method. The textures are not perfectly restored, but they are sufficiently present in the image to allow their reconstruction using the algorithm proposed in this paper.

Finally, if $\tilde{\xi}$ is known, by using Eqn. (10) and (11), the estimate for the coefficient is:

$$\hat{\xi} = \frac{|\tilde{\xi}|^2}{|\tilde{\xi}|^2 + 2\sigma_k^2} x \quad (12)$$

D. Noninformative Jeffrey's hyperprior

The most difficult problem in this approach is to get an approximation $\tilde{\xi}$ as close as possible to the original image coefficients.

The method RHEA used to obtain such an approximation is certainly not perfect and some residual noise remains. It is visible in constant areas. Then we need to put a prior distribution on the unknown variance parameters s^2 if we want them to make sense when estimated by MLE from noisy coefficients.

An approach consisting of taking Jeffrey's hyperprior has been proposed in [10] within a wavelet based image denoising framework. It is based on the following assumption: the inference procedure should be invariant under changes of amplitude and scale. It means that the prior probability density of s^2 must keep the same behaviour even if it is rescaled, by setting for example $s' = ks$. Since this is not the case for classical Gaussian or Laplacian models, the author uses the following prior, which is called a noninformative prior [2]:

$$P(s^2) \propto \frac{1}{s^2} \quad (13)$$

This corresponds to an extremely heavy-tailed distribution. Unfortunately it is improper: the density function is not integrable. However, the marginal density of the wavelet coef-

ficients is not improper.

We denote by η the transform coefficients corresponding to the image deconvolved using regularization (by RHEA for instance). In addition to the computation of the deconvolved noise variance $2\sigma_k^2$, we also need to compute the variances $2\tilde{\sigma}_k^2$ of the residual noise which corrupts the coefficients η .

The estimation of $\tilde{\xi}$ is then performed in two steps:

- estimate the variance \hat{s}^2 by using the MAP: $\hat{s}^2 = \arg \max_{s^2} P(s^2 | \eta)$
- estimate the unknown coefficient by using the MAP: $\tilde{\xi} = \arg \max_{\xi} P(\xi | \eta)$

To express $P(s^2 | \eta)$, we need $P(\eta | s^2)$ and $P(s^2)$. Since both signal and noise are Gaussian, of respective variances s^2 and $\tilde{\sigma}_k^2$, we have $P(\eta | s^2) = P(\eta_r | s^2)P(\eta_i | s^2)$. Then $P(\eta_r | s^2) = P(\eta_i | s^2) = N(N(0, s^2), \tilde{\sigma}_k^2) = N(0, s^2 + \tilde{\sigma}_k^2)$. We also have the hyperprior (13). Then we obtain:

$$\hat{s}^2 = \arg \max_{s^2} P(s^2 | \eta) \propto \frac{1}{(s^2 + \tilde{\sigma}_k^2)^2} e^{-|\eta|^2/2(s^2 + \tilde{\sigma}_k^2)}$$

which gives:

$$\hat{s}^2 = \begin{cases} |\eta|^2/4 - \tilde{\sigma}_k^2 & \text{if } |\eta|^2 \geq 4\tilde{\sigma}_k^2 \\ 0 & \text{if } |\eta|^2 < 4\tilde{\sigma}_k^2 \end{cases} \quad (14)$$

The MAP estimate $\tilde{\xi} = \arg \max_{\xi} P(\xi | \eta)$ for the adaptive Gaussian model is given by Eqn. (10). By combining equations (14) and (10) we obtain the following estimate, which we call the noninformative thresholding function θ_J :

$$\tilde{\xi} = \theta_J(\eta) = \frac{|\eta|^2 - 4\tilde{\sigma}_k^2}{|\eta|^2} \eta \quad \text{if } |\eta|^2 \geq 4\tilde{\sigma}_k^2, \quad 0 \text{ elsewhere} \quad (15)$$

The advantage of such a method is that there is no need for parameter estimation, since there is no parameter.

The thresholding function θ_J could be applied directly on the noisy coefficients obtained from the roughly deconvolved image, thus providing a simple and automatic deconvolution algorithm. However, there is a major drawback, which is especially visible in homogeneous areas: the residual noise is quite apparent, its variance being higher than with the previously presented homogeneous model. This probably comes from the lack of robustness of

the estimation method. We can remark that if we remove the prior law of s^2 , the estimation of s^2 is done by the MLE, which gives a function like (14) but with a threshold $2\tilde{\sigma}_k^2$ instead of $4\tilde{\sigma}_k^2$. This is insufficient since the magnitude of the noise has a variance equal to $2\tilde{\sigma}_k^2$. Thus, the hyperprior makes the estimation more robust, by doubling the threshold value. It is still not sufficient to remove noise peaks in large constant areas.

In the case of denoising an image deconvolved with regularization, as with RHEA, the robustness of this method is sufficient, since the level of the residual noise is quite small compared to the deconvolved noise. That is why we use the noninformative thresholding to estimate the approximate original coefficients $\tilde{\xi}$ from η , before using them to estimate the variance parameters s^2 from the complete data $\tilde{\xi}$. Finally, $\hat{\xi}$ is obtained from x using the estimated parameters s^2 . In the next section, we describe this procedure more precisely.

IV. THE DECONVOLUTION ALGORITHM

The adaptive model described by Eqn. (8) provides better results (visually and w.r.t. SNR) than the homogeneous model described by Eqn. (7). Details are better preserved and constant areas are cleaner [16]. We have also compared this scheme with the classical minimax approach [8] and with minimum risk computation for various models [16]. It consistently exhibits better results.

The initial deconvolution is made in the Cosine Transform space instead of the Fourier space to avoid artefacts near the borders of the image. The proposed algorithm is called COWPATH, for *COmplex Wavelet Packet Automatic THresholding*, and consists of the following steps (see Fig. 9):

- DCT (Discrete Cosine Transform) of the observation Y
- Deconvolution: divide by $\mathcal{F}[h]$ (in practice, divide by $\mathcal{F}[h] + \epsilon$ where ϵ is small, since some of the coefficients of $\mathcal{F}[h]$ can be null)
- Inverse DCT of the result, which gives X
- CWP transform of X
- Computation of σ_k using the known h and σ (see Eqn. (4))
- Computation of the approximate original image \tilde{X} : apply the RHEA algorithm [13] on Y (nonlinear regularization, with automatic parameter estimation)
- CWP transform of \tilde{X} to obtain η
- Computation of $\tilde{\sigma}_k$ (residual noise of the coefficients η) using the known h and σ (see

[16] for details)

- Thresholding of the approximate image coefficients using Jeffrey’s noninformative prior and $\tilde{\sigma}_k$ (see Eqn. (15))
- Estimation of the parameters \hat{s} of the inhomogeneous Gaussian model (see Eqn. (11))
- Coefficient thresholding by computing the MAP (see Eqn. (12))
- Set to zero the subbands where the variance of the noise is greater than the variance of the signal
- Inverse CWP transform, which gives the estimate \hat{X} .

The variance of the residual noise in homogeneous areas, which is needed to denoise the approximate original image before using this image for parameter estimation, is computed in the same manner as the variance of the deconvolved noise (i.e. using an equation similar to Eqn. (4), in which the denominator takes into account the regularization process). For this computation, we assume that constant regions correspond to a quadratic regularization. Then it is possible to use sums in the Fourier space. We refer to [16] for more details.

The main characteristic of this algorithm is the use of two different methods, regularization and wavelet thresholding, to obtain a hybrid technique whose results are better than the results of a single regularization method or a wavelet thresholding. The more decorrelated the deconvolved noise and the residual noise of the approximate original image, the higher the quality of the deconvolved image.

It is possible to replace the nonquadratic regularizing model of the RHEA algorithm by a simple quadratic model. The advantages are to enable a single step deconvolution in the frequency space and to make the parameter estimation step deterministic and fast (in the nonquadratic case we need a MCMC method [13]). The edges are not as sharp as with the nonquadratic model, but this approximate image is sufficiently accurate to provide a correct estimation of the inhomogeneous parameters of the subband model (the SNR difference between the original and accelerated algorithms is about 0.1 dB for the SPOT 5 simulation image shown in Fig. 13).

The complexity of the algorithm is computed as follows. We do not take into account the approximate original image, supposing it is provided. We have 3 DCT and 3 CWPT, which corresponds to about $15 \log_2 n + 500$ op/pix (i.e. operations per pixel) (650 op/pix for a 1024×1024 image). If the approximation discussed above is used, this is almost the total cost of the whole deconvolution algorithm.

V. SATELLITE IMAGE DEBLURRING

A. Results : SPOT 5 simulation

Fig. 10 shows a 128x128 area extracted from the original image of Nîmes (SPOT 5 simulation at 2.5 m resolution, provided by the French Space Agency (CNES)). Fig. 11 shows the PSF and Fig. 12 shows the observed image Y ($\sigma = 1.4$ and SNR=14.8 dB). Fig. 13 shows the image deconvolved with the proposed algorithm (SNR=20.9 dB), exhibiting sharp and regular oriented features, and noise-free constant areas.

B. Comparison with different methods

1. Quadratic regularization [28].

The quadratic regularization is nearly equivalent to the parametric Wiener filter [12], and gives the same results. It is also equivalent to isotropic diffusion. The edges are filtered as well as the noise, as seen on Fig. 14. It is therefore impossible to obtain sharp details and noise-free homogeneous areas at the same time. Thus, the SNR remains low (about 19.5 dB) because of insufficient noise removal in these areas.

2. Nonquadratic regularization [4], [11].

The resulting image of the RHEA algorithm [13] exhibits sharp edges, compared to the result shown previously. However, some noise remains in homogeneous regions and textures are attenuated. The SNR is 20.5 dB. This result is used as the approximate original image and is illustrated by Fig. 15.

3. Real wavelet packets, soft thresholding[17].

The proposed wavelet packet transform is more than two times faster than the shift invariant real wavelet packet transform (based on Symmlet-4 wavelets) and is much more directionally selective. Real wavelet packet soft thresholding gives a SNR equal to 19.6 dB (see Fig. 17) while the same type of thresholding using the CWPT provides a higher SNR and a higher quality image (see Fig. 16). In this experiment, the threshold is chosen manually, equal to α times the standard deviation of the deconvolved noise. Here, a value of α close to 1 provides a nearly optimal SNR .

4. Complex wavelet packets, soft thresholding.

The proposed hybrid thresholding method provides a sharper restored image than simple soft thresholding, due to the adaptive approach. To illustrate this, we show on Fig. 16 the result using a manually chosen threshold equal to α times the standard deviation

of the magnitude of the noise (a soft thresholding function is applied to each coefficient magnitude, without modifying the phase). We set $\alpha = 1$ as with real wavelets, which gives a nearly optimal SNR. In this case, we obtain a SNR equal to 19.9 dB.

VI. CONCLUSION

We have proposed a new complex wavelet packet transform to construct an efficient satellite image deconvolution algorithm. This transform exhibits better directional and shift invariance properties than real wavelet packet transforms, for a lower computational cost.

The proposed deconvolution method is superior to other competing algorithms on satellite images: it is faster, more accurate and fully automatic. The essential novelty of the proposed algorithm consists of an hybrid approach, in which two radically different methods are combined to produce a deconvolved image of higher quality than the result of each method individually. Finally, if a quadratic model is used, the speed is greatly increased, which opens the path to real time processing of image sequences or to onboard image processing in satellites by using specialized chips.

In this paper, we show results on a particular case (simulation of a SPOT 5-style satellite image). Tests have been performed with different types of blurs and various noise levels, and the proposed algorithm has shown its efficiency in most of the experiments. However, in some cases the rough deconvolution step is not adapted to the blurring kernel: if there are zeros in the transfer function, the noise amplification is too high, and the signal becomes difficult to recover. In such cases, the wavelet packet decomposition tree should be adapted to the noise statistics, thus enabling the covariance matrix of the noise to be nearly diagonal.

The case of noninvertible blur, such as motion blur, forbids the use of nonregularized inversion in the Fourier domain. Therefore, in this case, a regularized deconvolution should replace the rough inversion used in the proposed method.

An improvement of the adaptive Gaussian model could also be provided by choosing a more accurate distribution, to capture the heavy-tailed distribution of the wavelet packet coefficients. For example, adaptive Generalized Gaussian models could be investigated. Furthermore, including dependence between different scales by means of multiscale hidden Markov trees could help separating the small features from the deconvolved noise. These types of models would certainly better model edges which propagate across scales and

enable their reconstruction more efficiently.

VII. ACKNOWLEDGEMENTS

The authors would like to thank Jérôme Kalifa (from CMAPX, at Ecole Polytechnique) for interesting discussions and Nick Kingsbury (from the Signal Processing Group, Dept. of Eng., University of Cambridge) for the complex wavelets source code and collaboration, Peter de Rivaz (same institution) for his kind remarks, and the French Space Agency (CNES) for providing the image of Nîmes.

REFERENCES

- [1] M. Belge and E. Miller. Wavelet domain image restoration using edge preserving prior models. In *IEEE Proc. of ICIP*, Chicago, USA, Oct. 1998.
- [2] J. Bernardo and A. Smith. *Bayesian Theory*. John Wiley and Sons, Chichester, UK, 1994.
- [3] S.G. Chang and M. Vetterli. Spatial adaptive wavelet thresholding for image denoising. In *Proc. of ICIP*, Oct. 1997.
- [4] P. Charbonnier, L. Blanc-Féraud, G. Aubert, and M. Barlaud. Deterministic Edge-Preserving Regularization in Computed Imaging. *IEEE Trans. on IP*, 6(2):298–311, Feb. 1997.
- [5] R. Coifman and D. Donoho. Translation-invariant de-noising. Technical Report 475, Stanford University, 1995.
- [6] R. Coifman, Y. Meyer, and M. Wickerhauser. *Wavelets and their applications*, chapter Wavelet analysis and signal processing, pages 153–178. John and Barlett, 1992.
- [7] D. Donoho. Denoising by soft thresholding. *IEEE Trans on IT*, 41:613–627, 1995.
- [8] D. Donoho. Nonlinear solution of linear inverse problems by wavelet-vaguelette decomposition. *App. and Comp. Harmonic Analysis*, 2:101–126, 1995.
- [9] D. Donoho and I. Johnstone. Ideal spatial adaptation via wavelet shrinkage. *Biometrika*, 81:425–455, 1994.
- [10] M. Figueiredo and R. Nowak. Bayesian wavelet-based image estimation using noninformative priors. In *Proc. of the SPIE Conf. on Mathematical Modeling, Bayesian Estimation, and Inverse Problems*, Denver, USA, Jul. 1999.
- [11] S. Geman and D. Geman. Stochastic Relaxation, Gibbs Distributions and the Bayesian Restoration of Images. *IEEE Trans. on PAMI*, 6(6):721–741, Nov. 1984.
- [12] C. W. Helstrom. Image restoration by the method of least squares. *J. Opt. Soc. Amer.*, 1967.
- [13] A. Jalobeanu, L. Blanc-Féraud, and J. Zerubia. Hyperparameter estimation for satellite image restoration by a MCMCML method. In Springer, editor, *LNCS - EMMCVPR*, York, July 1999.
- [14] A. Jalobeanu, L. Blanc-Féraud, and J. Zerubia. Estimation of adaptive parameters for satellite image deconvolution. In *Proc. of ICPR*, Barcelona, Spain, Sept. 2000.
- [15] A. Jalobeanu, L. Blanc-Féraud, and J. Zerubia. Satellite image deconvolution using complex wavelet packets. In *Proc. of ICIP*, Vancouver, Sept. 2000.
- [16] A. Jalobeanu, L. Blanc-Féraud, and J. Zerubia. Satellite image deconvolution using complex wavelet packets. *INRIA Research Report 3955*, www.inria.fr/RRRT/RR-3955.html, June 2000.
- [17] J. Kalifa. Restauration minimax et déconvolution dans une base d'ondelettes miroirs. *Thèse de Doctorat, Ecole Polytechnique, France*, 1999.
- [18] J. Kalifa and S. Mallat. Wavelet packet deconvolutions. Technical report, CMAP, Ecole Polytechnique, Palaiseau, France, 1998.
- [19] N. Kingsbury. The dual-tree complex wavelet transform: a new efficient tool for image restoration and enhancement. In *Proc. of EUSIPCO*, pages 319–322, Rhodes, Greece, 1998.
- [20] N. Kingsbury. Image processing with complex wavelets. In *Phil. Trans. Roy. Soc. London A*, volume 357, pages 2543–2560, Special issue for the discussion meeting on "Wavelets: the key to intermittent information?" (held Feb. 24-25, 1999), Sept. 1999.
- [21] N. Kingsbury. Complex wavelet for shift invariant analysis and filtering of signals. *Journal of Appl. Comp. and Harm. Anal.*, 10(3):234–253, 2001.
- [22] M. Malfait and D. Roose. Wavelet-based image denoising using a markov random field a priori model. *IEEE Trans. on IP*, 6:549–565, Apr. 1997.
- [23] S. Mallat. A theory for multiresolution signal decomposition: the wavelet representation. *IEEE Trans. on PAMI*, 11(7):674–693, Jul. 1989.

- [24] P. Moulin. A wavelet regularization method for diffuse radar-target imaging and speckle-noise reduction. *Journal of Mathematical Imaging and Vision*, 3(1):123–134, 1993.
- [25] B. Rougé. Fixed Chosen Noise Restoration. *IEEE 95 Philadelphia, USA*, 1995.
- [26] L-I. Rudin, S. Osher, and E. Fatemi. Nonlinear total variation noise removal algorithm. *Physica D*, 60:259–268, 1992. Elsevier.
- [27] E. Simoncelli. Bayesian denoising of visual images in the wavelet domain. In P. Muller and B. Vidakovic, editors, *Bayesian inference in wavelet-based methods*. Springer Verlag, 1999.
- [28] A.N. Tikhonov. Regularization of incorrectly posed problems. *Sov. Math. Dokl.*, 4:1624–1627, 1963.

Satellite image deblurring using complex wavelet packets

André Jalobeanu, Laure Blanc-Féraud, Josiane Zerubia

IJCV

Figures

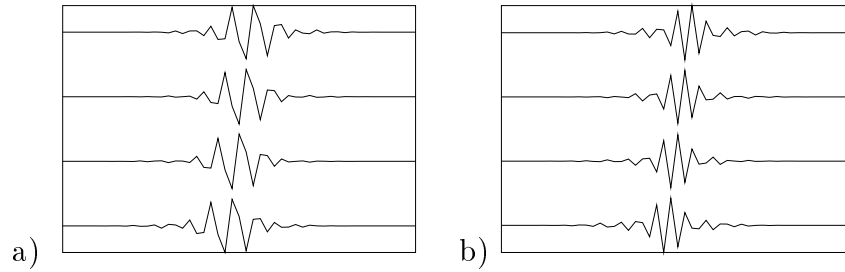


Fig. 1. We consider the 1D CWP transform. This figure illustrates the approximate shift invariance, by showing a shifted step function filtered by setting to zero all the subbands excepted one packet subband. 4 different shifts are represented (1, 2, 3 and 4 sampling units) from bottom to top. a) Lowest frequency packets. b) Highest frequency packets.

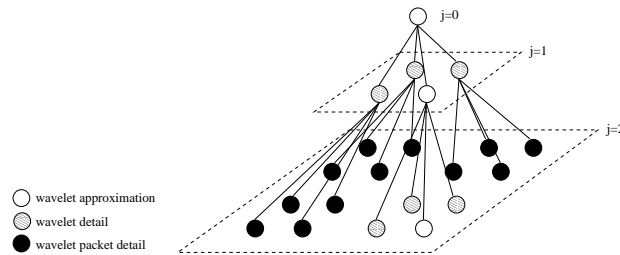


Fig. 2. Wavelet packet tree

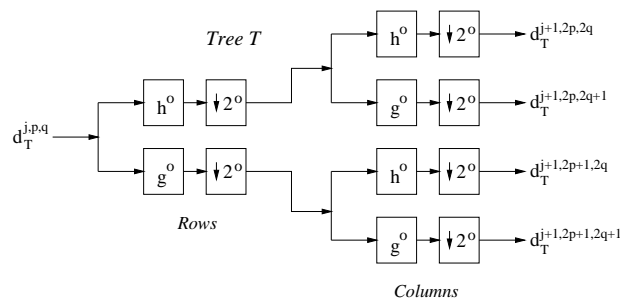


Fig. 3. One tree of the quad-tree filter bank

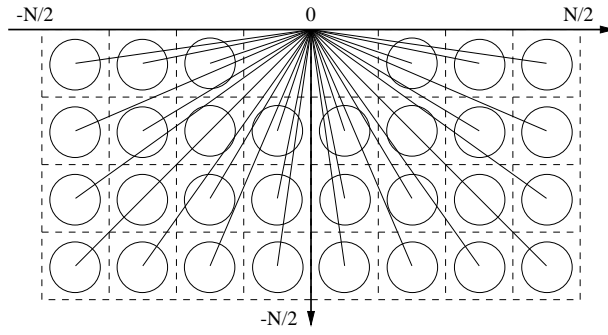


Fig. 4. Rough partition of the frequency plane induced by the CWPT

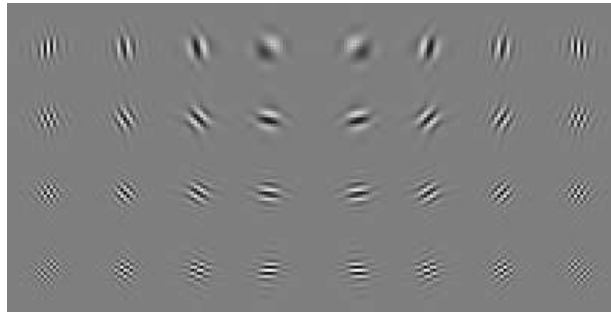


Fig. 5. Impulse responses of the CWPT at level 2 (real part) - left : z_+ , right : z_-

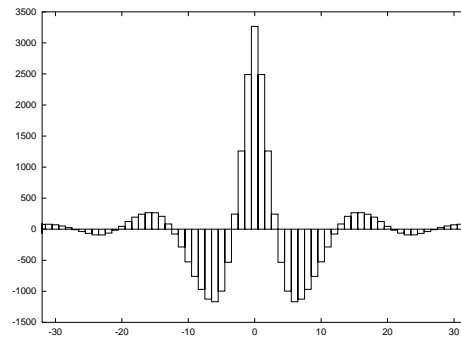


Fig. 6. Real part of the covariance of the deconvolved noise (w.r.t. columns) for one complex wavelet subband

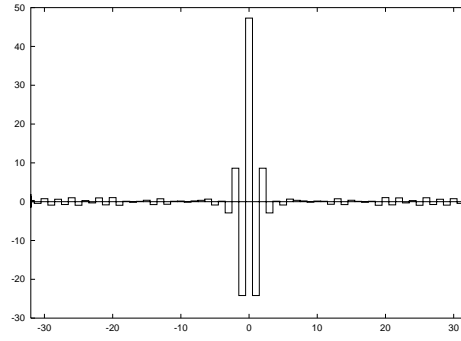


Fig. 7. Real part of the covariance of the deconvolved noise (w.r.t. columns) for one complex wavelet *packet* subband

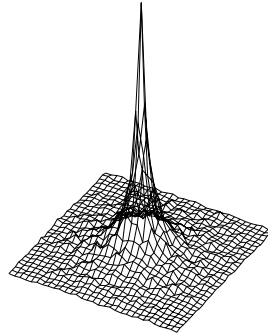


Fig. 8. Distribution $P(\xi)$ of CWP coefficients of the original image, for one packet subband

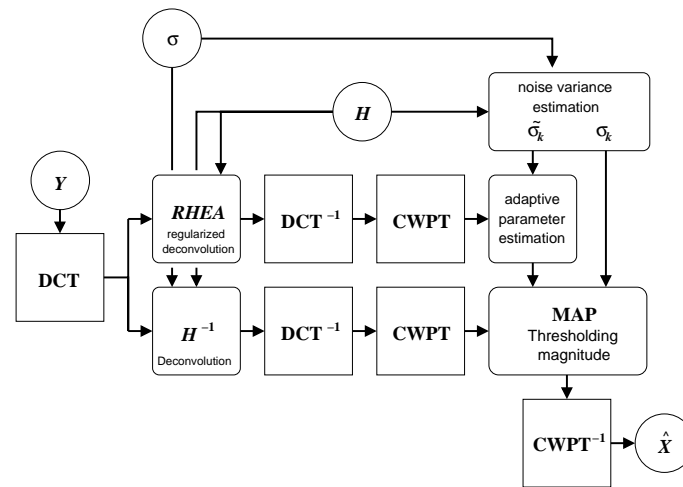


Fig. 9. The COWPATH algorithm



Fig. 10. Original image \mathcal{X} (128x128 area extracted from Nîmes)

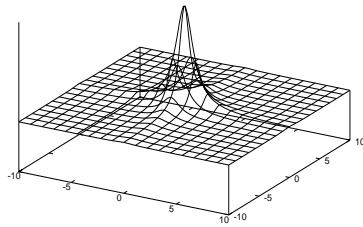


Fig. 11. Point Spread Function (PSF) h



Fig. 12. Observed image Y (SNR=14.8 dB)



Fig. 13. Image deconvolved with the proposed method (SNR=20.9 dB)



Fig. 14. Image deconvolved with quadratic regularization (SNR=19.5 dB)



Fig. 15. Image deconvolved with nonquadratic regularization (SNR=20.5 dB)



Fig. 16. Image deconvolved using complex wavelet packets and soft thresholding (SNR=19.9 dB)



Fig. 17. Image deconvolved using real wavelet packets and soft thresholding (SNR=19.6 dB)